THEORETICAL STUDY ON THE MECHANISM OF REACTION OF GROUND-STATE Fe ATOMS WITH CARBON DIOXIDE

Dimitrios A. PANTAZIS[1], Athanassios C. TSIPIS[2] and Constantinos A. TSIPIS[3,*]

Laboratory of Applied Quantum Chemistry, Faculty of Chemistry, Aristotle University of Thessaloniki, 541 24 Thessaloniki, Greece; e-mail: [1] dp25@york.ac.uk, [2] tsipis@chem.auth.gr, [3] tsipis@chem.auth.gr

Received May 21, 2003
Accepted August 11, 2003

Dedicated to Professor Rudolf Zahradník on the occasion of his 75th birthday.

Density functional calculations at the B3LYP level of theory, using the 6-31G(d) and 6-311+G(3df) basis sets, provide a satisfactory description of the geometric and energetic reaction profile of the Fe + CO_2 → FeO + CO reaction. The reaction is predicted to be endothermic by 23.24 kcal/mol at the B3LYP/6-311+G(3df)//B3LYP/6-31G(d) level of theory and to proceed by formation of either a Fe(η^2-**OC**O) or a Fe(η^3-**OCO**) intermediate. The Fe(η^2-**OC**O) intermediate in the $^5A'$ ground state is weakly bound with respect to Fe(^{5}D) and CO_2 dissociation products by 0.78 (2.88) kcal/mol at the B3LYP/6-31G(d) (B3LYP/6-311+G(3df)//B3LYP/6-31G(d)) levels of theory. In contrast, the Fe(η^3-**OCO**) intermediate in the $^5A_1$ ground state is unbound with respect to Fe(^{5}D) and CO_2 dissociation products by 8.27 (11.15) kcal/mol at the same levels of theory. However, both intermediates are strongly bound relative to the separated Fe^+(^{6}D) and $[CO_2]^-$ anion; the computed bond dissociation energies for the Fe(η^2-**OC**O) and Fe(η^3-**OCO**) intermediates are 207.33 and 198.28 kcal/mol in terms of ΔE_0 at the B3LYP/6-31G(d), respectively. In the Fe(η^2-**OC**O) and Fe(η^3-**OCO**) intermediates, an intramolecular insertion reaction of the Fe atom to O–C bond takes place yielding the isomeric OFe(η^1-**C**O) and OFe(η^1-**O**C) products, respectively, with a relatively low activation barrier of 25.24 (21.69) and 26.36 (23.38) kcal/mol at the B3LYP/6-31G(d) (B3LYP/6-311+G(3df)//B3LYP/6-31G(d)) levels of theory, respectively. The calculated structures, relative stability and bonding properties of all stationary points are discussed with respect to computed electronic and spectroscopic properties, such as charge density distribution and harmonic vibrational frequencies.

Keywords: DFT; $FeCO_2$ complexes; CO_2-to-CO reduction; Reaction mechanism; Electronic structure; *Ab initio* calculations; Iron.

The use of carbon dioxide as a renewable resource, *i.e.* the re-use of existing CO_2 as a source of carbon for producing chemicals is of great potential[1]. Utilization of CO_2 as a possible starting material for the synthesis of fine chemicals provides an attractive alternative to compounds presently de-

rived from coal and petroleum[2]. The activation of the thermodynamically and kinetically inert carbon dioxide molecule may be accomplished by photochemical, electrochemical or catalytic processes[3]. However, in all cases, the coordination of CO_2 on a metallic centre seems to be the key step for the ultimate reduction of CO_2 (refs[1,4]). The one-to-one transition metal–carbon dioxide complexes have been observed in net matrices and characterized as $M(CO_2)$ complexes using UV-VIS and FTIR spectroscopy[5]. Moreover, in recent years, gas-phase studies of complexes of the CO_2 molecule with transition metal ions have attracted considerable attention, since these complexes may serve as potential precursors for the challenging task of carbon dioxide fixation[6]. Some quantum chemical calculations for the neutral MCO_2 complexes[7–10] and the cationic $[MCO_2]^+$ molecules[11,12] with transition metals have also been reported. The geometry and binding interaction of CO_2 with the first-row transition metal cations have been studied using *ab initio* and density functional methods. On the other hand, restricted Hartree–Fock, configuration interaction and perturbation calculations were performed on the neutral MCO_2 of the first-row transition metals, except Fe, to establish the bond strength, the stable geometry, and the electron distribution of these molecules. When iron atoms are co-condensed with CO_2 in net matrices at 15 K, they form a $FeCO_2$ complex, which, according to the observed IR frequencies and isotopic shifts, involves probably a C-coordinated CO_2 ligand[5c]. Moreover, a more interesting point for iron is its apparent ability to reduce CO_2 to CO by thermal activation of the CO_2 matrix, which may occur by the reaction scheme:

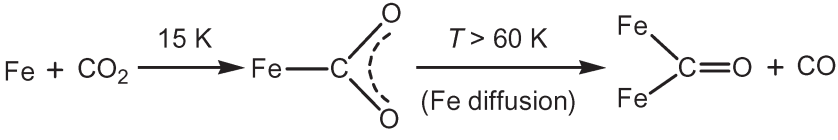

However, no detailed study of the Fe + CO_2 reaction mechanism has been reported so far. Therefore, we thought it would be advisable to carry out a detailed quantum chemical investigation of the Fe + CO_2 reaction mechanism in order to consider different coordination modes of the CO_2 ligand (η^3-**OCO**, η^2-**OC**O ("side-on"), η^2-O**CO**, η^1-**O**CO, and η^1-O**C**O), to the ground-state Fe metal center, and to explore the geometric and energetic profile of the CO_2-to-CO reduction reaction. Studies of the ligation modes of CO_2 to transition metal atoms could also act as guides to the biologically important photosynthesis and respiration processes.

COMPUTATIONAL DETAILS

The structural, electronic and energetic properties of all compounds were computed at the Becke three-parameter hybrid functional[13] combined with the Lee–Yang–Parr correlation functional[14] abbreviated as the B3LYP level of theory, using the 6-31G(d) basis set. Moreover, single-point energy calculations used the larger 6-311+G(3df) basis set. The hybrid B3LYP functional was used, since it has been applied extensively to inorganic problems, and the accuracy of the calculated energies has been demonstrated for a variety of systems, including organometallic compounds[15]. In all computations no constraints were imposed on the geometry. Full geometry optimization was performed for each structure using Schlegel's analytical gradient method[16], and the attainment of the energy minimum was verified by calculating the vibrational frequencies that result in the absence of imaginary eigenvalues. All the stationary points have been identified as minima (number of imaginary frequencies NIMAG = 0) or transition states (NIMAG = 1). The vibrational modes and the corresponding frequencies are based on a harmonic force field. This was achieved with the SCF convergence on the density matrix of at least 10^{-9} and the root mean square (RMS) of the force less than 10^{-4} a.u. All bond lengths and bond angles were optimized to better than 0.001 Å and 0.1°, respectively. The computed electronic energies, the enthalpies of reactions, $\Delta_R H_{298}$ and the activation Gibbs energies, $\Delta G^{\ddagger}_{298}$, were corrected to constant pressure and 298 K, for zero point energy (ZPE) differences and for the contributions of the translational, rotational and vibrational partition functions. For transition-state geometry determination, quasi-Newton transit-guided (QSTN) computations were performed[17]. Moreover, corrections of the transition states have been confirmed by intrinsic reaction coordinate (IRC) calculations, while intrinsic reaction paths (IRPs)[18] were traced from the various transition structures to make sure that no further intermediates exist. All calculations were performed using the Gaussian 98 series of programs[19]. Moreover, the qualitative concepts and the graphs derived from Chem3D program suite[20] highlight the basic interactions resulting from the DFT calculations.

RESULTS AND DISCUSSION

Coordination of CO_2 to Ground-State Fe Atoms

Two trajectories concerning the initial interaction between the ground state Fe(^{5}D) atom with the CO_2 molecule were considered: (i) approach of the Fe

atom to the C atom of the CO_2 molecule following a perpendicular trajectory (side-on approach) and (ii) approach of the Fe atom to the O end of the CO_2 molecule following a collinear trajectory (end-on approach). The potential energy curves for the two trajectories are depicted schematically in Fig. 1.

It can be seen that in both trajectories the Fe atom is weakly associated with the CO_2 molecule through London dispersion forces at an equilibrium distance of 4.487 and 4.106 Å for the side-on, **1**, and end-on, **2**, approaches, respectively; the computed association energies are 0.68 (1.03) and 0.50 (1.12) kcal/mol in terms of ΔE_0 (ΔH^0_{298}), respectively. Searching the poten-

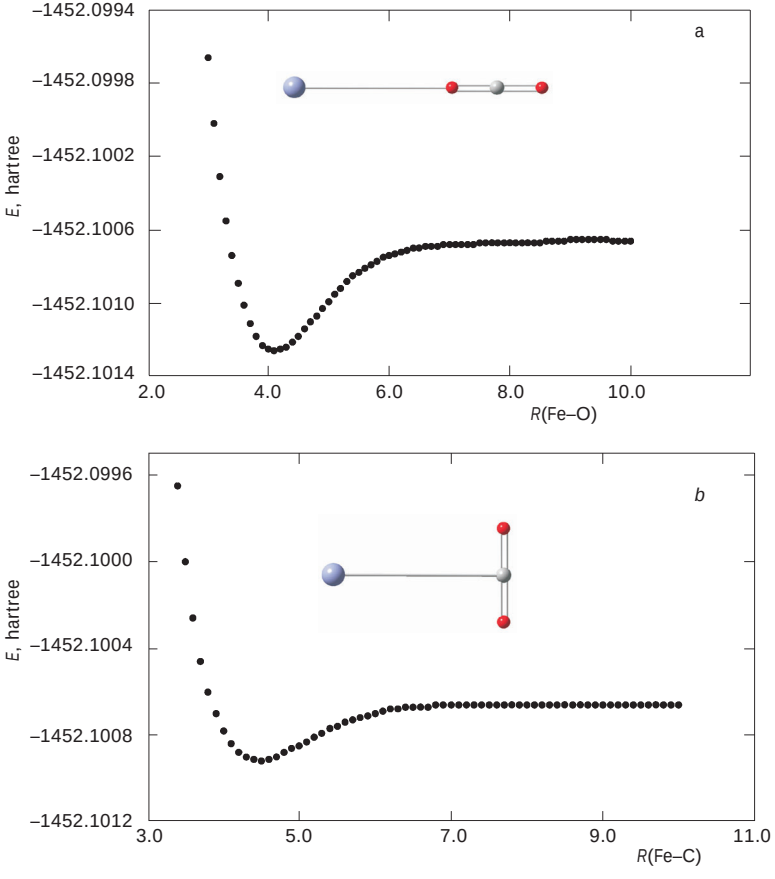

FIG. 1

Potential energy curves of the perpendicular trajectory (side-on approach) (a) and the collinear trajectory (end-on approach) (b) of the interaction of ground-state Fe atoms with CO_2 computed at the B3LYP/6-31G(d) level of theory

tial energy surface (PES) of the [$FeCO_2$] system we found local minima corresponding to stable $FeCO_2$ complexes as well as saddle points with equilibrium structures shown in Fig. 2. The first local minimum in the PES of the [$FeCO_2$] system corresponds to complex **3**, with the CO_2 ligand coordinated

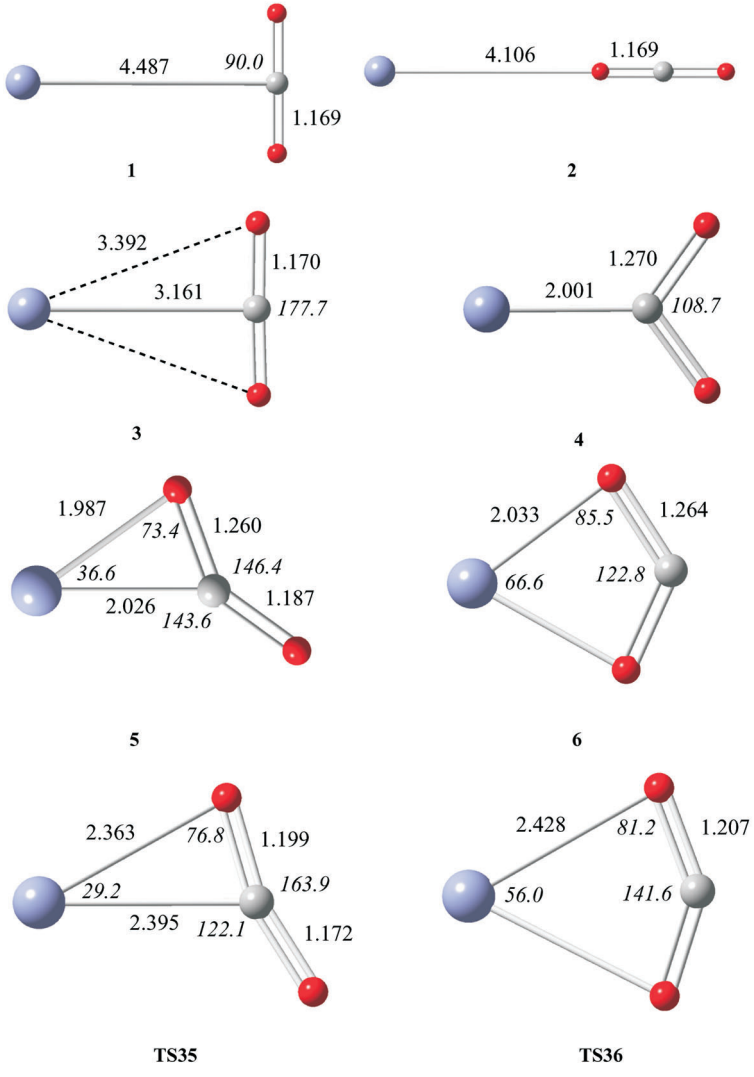

FIG. 2

Equilibrium structures (bond lengths in Å, bond angles in °) of the stationary points located on the PES of the [Fe,CO_2] system computed at the B3LYP/6-31G(d) level of theory

to Fe atom in the η^1-O**C**O bonding mode. This side-on complex belonging to the C_{2v} point group implies a $^5A_1$ state correlating to the CO_2 ($^1\Sigma_g^+$) ground state and the Fe(^{5}D) ground atomic state generated by the $3d^64s^2$ configuration, while the electron configuration of the unpaired electrons is $(b_1)^1(b_2)^1(a_1)^1(a_1)^1$. The Fe–C bond length, 3.161 Å, is much shorter than that of the loose adduct **1** formed at the entrance channel by 1.326 Å. However, even at this distance the interaction of CO_2 with Fe is very weak, the complex **3** being stabilized with respect to adduct **1** by 0.58 (3.12) kcal/mol at the B3LYP/6-31G(d) (B3LYP/6-311+G(3df)//B3LYP/6-31G(d)) levels of theory, respectively. As a result of the weak interactions, the changes in the geometrical parameters of the CO_2 ligand are very small; the C–O bond is elongated by about 0.001 Å, while the linear CO_2 ligand is slightly bent by 2.3°. There is a small charge transfer of 0.02 charge units of natural charge from the Fe atom towards the C atom of CO_2. Moreover, there are very weak bonding orbital interactions between the d_{xz} AO of Fe with the π^*-MO of CO_2 described by the HOMO-3 (**3**) (Scheme 1) at –10.15 eV. The total spin density is accumulated on the Fe atom (Scheme 1) in **3** with the $\langle S^2 \rangle$ value of 6.006 indicating minimal artificial spin contamination in the calculations.


HOMO-3 (**3**)


Spin Density (**3**)


Spin Density (**4**)


Spin Density (CO_2^-)


HOMO-5 (**4**)


HOMO-6 (**4**)


HOMO-7 (**4**)


HOMO-8 (**4**)


HOMO-5 (**5**)

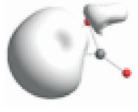
Spin Density (**5**)


HOMO-6 (**6**)


HOMO-7 (**6**)


HOMO-8 (**6**)


Spin Density (**6**)

SCHEME 1

The η^1-O**C**O bonding mode of ligation was also identified in complex **4** of C_{2v} symmetry corresponding to a second local minimum in the PES of the [$FeCO_2$] system at 62.17 (55.31) kcal/mol higher in energy than **3** in terms of ΔE_0 at the B3LYP/6-31G(d) (B3LYP/6-311+G(3df)//B3LYP/6-31G(d)) levels. In contrast to complex **3**, there are significant structural changes on the ligated CO_2 molecule in complex **4**. The C–O bonds are stretched to 1.270 Å while the O–C–O bond angle changes from 180.0 to 108.7°. This distortion is stronger than in isolated $[CO_2]^-$ anion exhibiting the C–O bond length of 1.253 Å and O–C–O bond angle of 133.7° at the same level of theory. The Fe–C bond length of 2.001 Å is much shorter than those of complexes **1** and **3**. Complex **4** in its $^5B_1$ ground state is unbound with respect to Fe(^{5}D) and CO_2 dissociation products by 61.10 (52.18) kcal/mol at the B3LYP/6-31G(d) (B3LYP/6-311+G(3df)//B3LYP/6-31G(d)) levels, but it is strongly bound relative to the separated Fe^+(^{6}D) and $[CO_2]^-$ anion; the computed bond dissociation energy is 145.09 kcal/mol in terms of ΔE_0 at the B3LYP/6-31G(d) level. The electron configuration of the unpaired electrons is $(a_2)^1(a_1)^1(a_2)^1(a_1)^1$. The geometry distortion in complex **4** leads to significant charge redistributions. There is a charge transfer of 0.48 charge units of natural charge from the Fe atom towards the CO_2 ligand; the C donor atom acquires a positive natural charge of 0.33 charge units, while the O atoms acquire negative natural charge of –0.41 charge units. In the free $[CO_2]^-$ ligand, the C and O atoms acquire 0.53 and –0.77 charge units of natural charge, respectively. The total atomic spin densities on the Fe and O atoms are 3.02 and 0.54, respectively (Scheme 1), while the natural electron configuration of Fe is $4s^{1.20}3d^{6.30}$. In the free $[CO_2]^-$ ligand, the total atomic spin densities on the C and O atoms are 0.68 and 0.16, respectively (Scheme 1). Moreover, there exist bonding orbitals between the Fe and the CO_2 ligand in complex **4** corresponding to HOMO-5, HOMO-6, HOMO-7, and HOMO-8 (Scheme 1).

The η^1-O**C**O complex **3** is easily converted either to the η^2-**OC**O, **5**, or η^3-**OCO**, **6**, complexes *via* transition states **TS35** and **TS36** surmounting an activation barrier of 4.38 (4.03) and 16.74 (15.13) kcal/mol, respectively at the B3LYP/6-31G(d) (B3LYP/6-311+G(3df)//B3LYP/6-31G(d)) levels of theory. The energetic and geometric profile of the Fe(η^1-O**C**O) (**3**) → Fe(η^2-**OC**O) (**5**) and Fe(η^1-O**C**O) (**3**) → Fe(η^3-**OCO**) (**6**) transformations is shown in Fig. 3. It can be seen that the Fe(η^1-O**C**O) → Fe(η^2-**OC**O) transformation is an almost barrierless process yielding the η^2-**OC**O complex, which corresponds to the global minimum in the PES. On the other hand, the η^3-**OCO** isomer corresponds to a local minimum at 9.05 (14.03) kcal/mol higher in energy than the global minimum. Note that all figures in parentheses are the computed

values at the B3LYP/6-311+G(3df)//B3LYP/6-31G(d) level of theory. Complex **6** in the $^5A_1$ ground state is unbound with respect to Fe(^{5}D) and CO_2 dissociation products by 8.27 (11.15) kcal/mol, but it is strongly bound relative to the separated Fe^+(^{6}D) and $[CO_2]^-$ anion; the computed bond dissociation energy is 198.28 kcal/mol in terms of ΔE_0 at the B3LYP/6-31G(d) level. Moreover, the electron configuration of the unpaired electrons is $(a_1)^1(a_2)^1(b_2)^1(a_1)^1$. In contrast, complex **5** in the $^5A'$ ground state is weakly bound with respect to Fe(^{5}D) and CO_2 dissociation products by only 0.78 (2.88) kcal/mol and also strongly bound relative to the separated Fe^+(^{6}D) and $[CO_2]^-$ anion; the computed bond dissociation energy is 207.33 kcal/mol in terms of ΔE_0 at the B3LYP/6-31G(d) level. The electron configuration of the unpaired electrons is $(a'')^1(a')^1(a')^1(a')^1$. For **6** a local minimum has also been identified in the PES at 3.29 kcal/mol higher in energy than the global minimum corresponding to the electromer with the $^5B_1$ electronic state and the electron configuration of the unpaired electrons $(a_2)^1(b_1)^1(b_2)^1(a_1)^1$. In

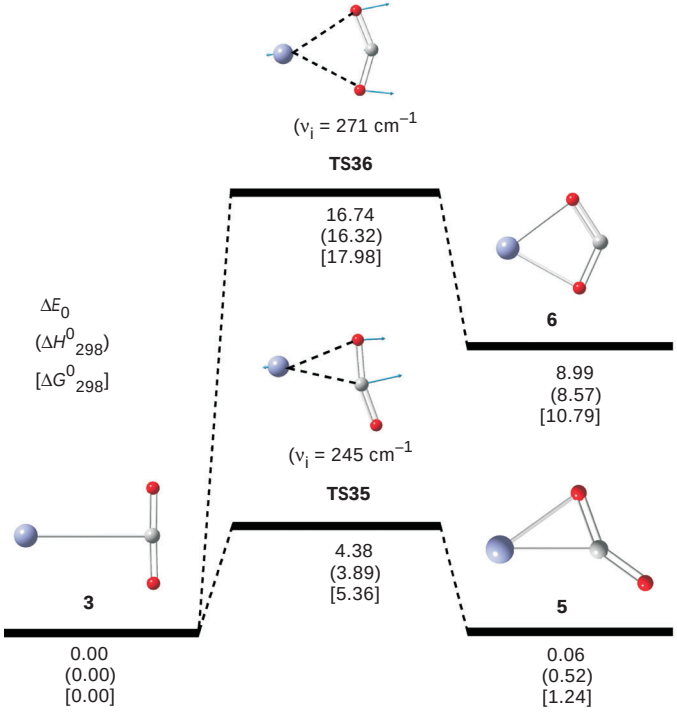

FIG. 3

The energetic and geometric profile of the Fe(η^1-O**C**O) (**3**) → Fe(η^2-**OC**O) (**5**) and Fe(η^1-O**C**O) (**3**) → Fe(η^3-**OCO**) (**6**) transformations (energies in kcal/mol) computed at the B3LYP/6-31G(d) level of theory

both complexes **5** and **6**, there are significant structural changes on the ligated CO_2 molecule. The C–O bonds are stretched to 1.260 and 1.264 Å, and the O–C–O bond angle changes from 180.0 to 146.4 and 122.8° in **5** and **6**, respectively. These distortions are very close to those of the isolated $[CO_2]^-$ anion. Obviously, complexes **5** and **6** can be considered as complexes formed upon interaction of the $Fe^+(^6D)$ cation with the bent $[CO_2]^-$ anionic ligand. The geometry distortions in complexes **5** and **6** introduce significant charge redistributions. There is a charge transfer of 0.53 charge units of natural charge from the Fe atom towards the CO_2 ligand in **5**; the C donor atom acquires a positive natural charge of 0.67 charge units, while the O atoms acquire negative natural charges of –0.70 and –0.49 charge units. There is a bonding σ(Fe–C) interaction between the Fe and C atoms (bond overlap population value of 0.169) constructed from an $sd^{1.71}$ hybrid (62.91% d-character) on Fe atom, $h_{Fe} = 0.5392(3d_{xy})_{Fe} + 0.5705(3d_{x^2-y^2})_{Fe}$, interacting with an $sp^{3.81}$ hybrid (79.08% p-character) on carbon atom, $h_C = -0.4302(2s)_C + 0.5687(3p_x)_C + 0.6800(3p_y)_C$, thus having the form $\sigma(Fe–C) = 0.6713h_{Fe} + 0.7412h_C$. The total atomic spin densities on the Fe and O atoms of complex **5** are 4.20 and 0.07, respectively (Scheme 1), while the natural electron configuration of Fe is $4s^{1.26}3d^{6.16}$. Moreover, most of the $Fe(CO_2)$ orbitals are pure Fe and CO_2 orbitals with only a slight admixture with the other moiety; however, the HOMO-5 corresponds to a bonding MO constructed from metal and ligand orbitals (Scheme 1).

There is a charge transfer of 0.26 charge units of natural charge from the Fe atom towards the CO_2 ligand in **6**; the C donor atom acquires a positive natural charge of 0.73 charge units, while the O atoms acquire negative natural charges of –0.73 charge units. The total atomic spin density on the Fe atom of **6** is 4.45 (Scheme 1), while the natural electron configuration of Fe is $4s^{1.17}3d^{6.04}$. In addition, there exist weak bonding orbital interactions described by the HOMO-6, HOMO-7 and HOMO-8 (Scheme 1), which are also reflected on the low Fe–O and Fe–C bond overlap population values of 0.0734 and 0.012, respectively, thus supporting the η^3-**OCO** bonding mode in **6**.

Both transition states **TS35** and **TS36** adopt a product-like structure with the CO_2 ligand coordinated to Fe atom in the η^2-**OC**O and η^3-**OCO** bonding mode, respectively. The imaginary frequencies at 245i and 271i cm^{-1} for **TS35** and **TS36**, respectively, correspond to the stretching of the respective bonds leading to the formation of the products. The normal coordinate vectors (arrows) of the vibrational modes are shown in Fig. 3. In **TS35** and **TS36** there is a charge transfer of about 0.17 and 0.04 charge units of natu-

ral charge from Fe to CO_2. Moreover, the total atomic spin densities on the Fe and O atoms of **TS35** and **TS36** are 4.05 and 0.02, and 3.77 and 0.47, respectively, while the natural electron configuration of Fe is $4s^{1.77}3d^{6.03}$ and $4s^{1.76}3d^{6.16}$, respectively.

Reforming CO_2 to CO by Ground-State Fe Atoms

The next goal of this work is the study of the mechanism of the reduction of CO_2 to CO by the ground-state Fe atoms. The Fe + CO_2 → FeO + CO reaction is found to be endothermic by 69.70 (23.24) kcal/mol. Based on the experimental heats of formation for Fe (99.30 kcal/mol), FeO (60.00 kcal/mol), CO_2 (–94.05 kcal/mol) and CO (–26.42 kcal/mol)[21], one can see that the Fe + CO_2 → FeO + CO reaction is endothermic by 28.33 kcal/mol. In general terms, the best estimate of the endothermicity of the reaction is that obtained using the larger basis set with *f* polarization functions. The total and ZPE-corrected energies of all stationary points found in the PES of the Fe + CO_2 → FeO + CO reaction computed at the B3LYP/6-311+G(3df)//B3LYP/6-31G(d) level of theory are summarized in Table I.

Two possible alternative reaction pathways were followed depending on the nature of the entrance channel, which could involve either the intermediate **5** or **6**. The energetic and geometric profiles of the two reaction pathways are depicted schematically in Fig. 4, while the equilibrium structures of the stationary points along the reaction pathways are shown in Fig. 5. It can be seen that in pathway (**a**) an intramolecular insertion reaction of the Fe atom into the O–C bond of intermediate **5** takes place yielding, *via* the transition state **TS57**, the product OFe(η^1-**C**O), **7**, with a relatively low activation barrier of 25.24 (21.69) kcal/mol. The structure of **7**, in the $^5A''$ ground state associated with the $(a')^1(a'')^1(a')^1(a')^1$ configuration for the unpaired electrons, corresponds to a η^1-**C**O-coordinated CO ligand to the Fe end of the FeO molecule in a slightly bent (O–Fe–C bond angle of 171.1°) bonding mode with the two O atoms in *anti*-configuration. A conformer with the *syn*-configuration of the two O atoms, **8**, was located as a saddle point in the PES (ν_i = 33 cm^{-1}) at 26.59 kcal/mol higher in energy at the B3LYP/6-31G(d) level. Product **7** can further dissociate to the FeO and CO products through an endothermic process by 29.34 (21.25) kcal/mol. The imaginary frequency of **TS57** at 395i cm^{-1} corresponds to the bending of the O=Fe–C moiety. The normal coordinate vectors (arrows) of the vibrational mode are shown in Fig. 4. **TS57** corresponds to a reactant-like transition state with some structural changes related to the elongation of the η^2-coordinated C–O bond by 0.611 Å, the shortening of the Fe–O and the terminal

C–O bonds by 0.268 and 0.028 Å, respectively, and the opening of the O–Fe–C bond angle by 25.8°. Summing up, the predicted low activation barrier for the reduction of CO_2 with ground-state Fe atoms is in line with the experimental results that the Fe atoms give rise, upon annealing above 80 K, to CO_2 reduction to CO along with the simultaneous formation of metal carbonyl complexes[5c]. However, the proposed reaction scheme for the reduction process involving formation of a bent Fe(η^1-O**C**O) complex[5c] could not be verified by our calculations, since the analogous Fe(η^1-O**C**O)

TABLE I
Total energies (in hartrees), ZPE (in kcal/mol)[a] and ZPE-corrected relative energies (in kcal/mol) of all stationary points found in the PES of the Fe + CO_2 → FeO + CO reaction computed at the B3LYP/6-311+G(3df)//B3LYP/6-31G(d) level of theory

	Total energy	ZPE	Rel. energy
Fe	–1263.641112		
CO_2	–188.659994	7.27	
Fe + CO_2	**–1452.301106**	**7.27**	**0.00**
1	–1452.301116	7.29	–0.01
2	–1452.300964	7.33	0.01
3	–1452.306088	7.27	–3.13
4	–1452.216037	6.07	52.18
5	–1452.306101	7.02	–2.88
TS35	–1452.299672	6.59	0.22
6	–1452.281979	6.41	11.15
TS36	–1452.276963	6.12	15.00
7	–1452.294906	5.37	1.99
TS37	–1452.268435	5.58	18.81
FeO	–1338.903420	1.44	
CO	–113.356391	3.16	
FeO + CO	–1452.259811	4.60	23.24
9	–1452.249932	5.38	30.22
TS69	–1452.244711	5.03	33.15
10	–1452.263643	5.45	21.69
TS910	–1452.246520	4.94	31.92
TS107	–1452.263419	5.02	23.65

[a] ZPE vibrational energy corrections were taken from the B3LYP/6-31G(d) calculations.

complex, **4**, is much higher in energy than the Fe(η^2-**OC**O) intermediate, **5**, corresponding to the global minimum. In effect, the reduction process proceeds through the Fe(η^2-**OC**O) intermediate, **5**. It is worth noting that a similar barrierless reaction pathway for the reduction of CO_2 to CO with Sc atoms involving the formation of a Sc(η^2-**OC**O) intermediate has been proposed very recently by Hwang and Mebel[9].

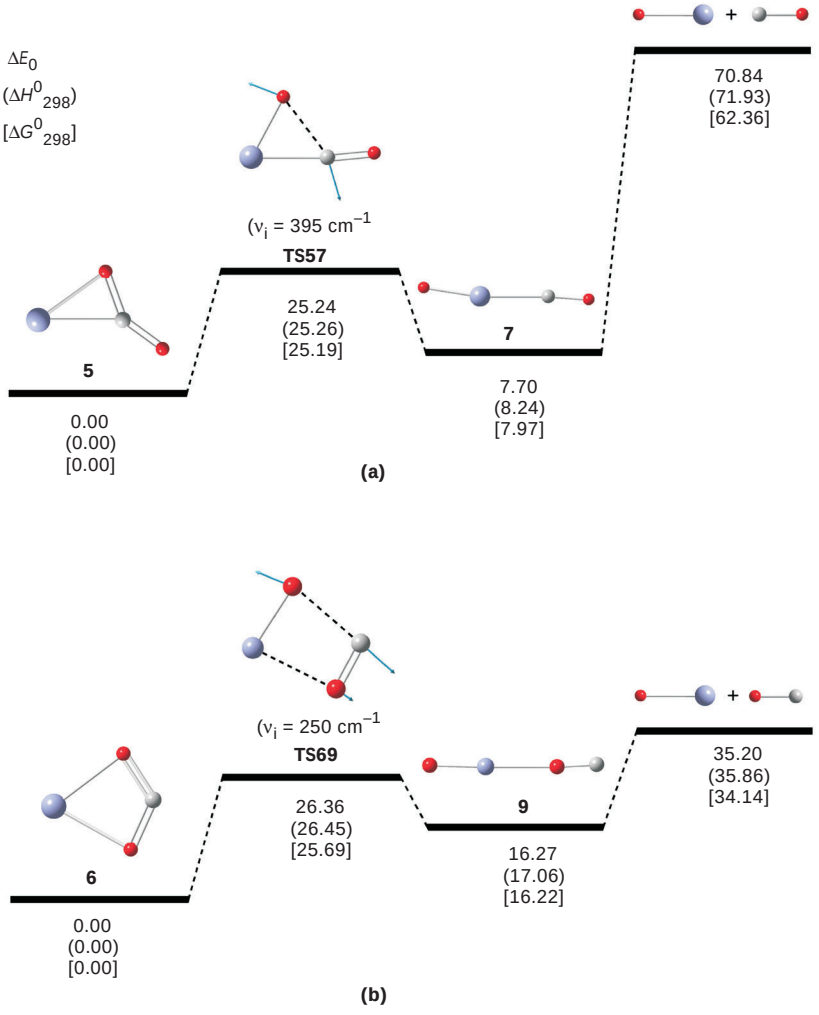

FIG. 4

The energetic and geometric profile of the Fe + CO_2 → FeO + CO reaction (energies in kcal/mol) for the two possible reaction pathways (**a**) and (**b**) computed at the B3LYP/6-31G(d) level of theory

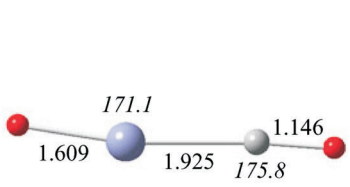

7

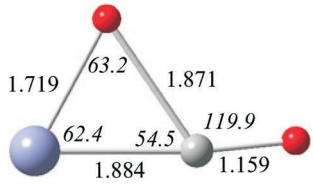

TS57

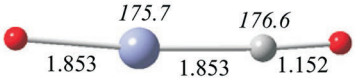

8

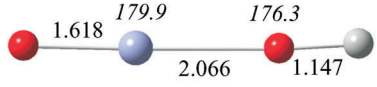

9

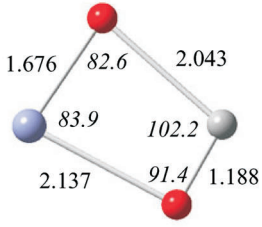

TS69

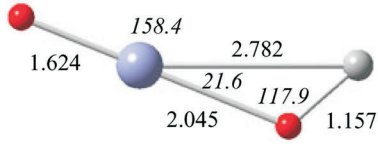

TS910

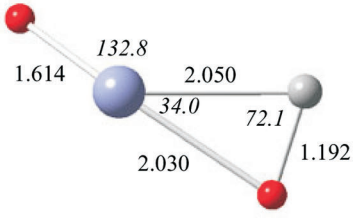

10

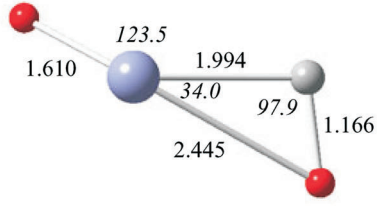

TS107

FIG. 5

Equilibrium structures (bond lengths in Å, bond angles in °) of the stationary points located on the PES of the [Fe,CO_2] system computed at the B3LYP/6-31G(d) level of theory

The alternative reaction pathway (**b**) starting with the Fe(η^3-**OCO**) intermediate, **6**, involves also an intramolecular insertion reaction of the Fe atom into the O–C bond yielding, *via* the transition state **TS69**, the isomeric product OFe(η^1-**O**C), **9**, with a relatively low activation barrier of 26.36 (23.38) kcal/mol. The structure of **9**, in the ^{5}A′ ground state associated with the $(a')^1(a'')^1(a'')^1(a')^1$ configuration for the unpaired electrons, corresponds to an η^1-**O**C-coordinated CO ligand to the Fe end of the FeO molecule in an almost linear (Fe–O–C bond angle of 176.3°) bonding mode. Product **9** can further dissociate to the FeO and CO products through an endothermic process by 18.93 (6.98) kcal/mol. The imaginary frequency of **TS69** at 250i cm^{-1} corresponds to the stretching of the Fe–O and the adjacent C–O bond. The normal coordinate vectors (arrows) of the vibrational mode are shown in Fig. 4. **TS69** corresponds to a reactant-like transition state with some structural changes related to the shortening of one of the Fe–O bonds by 0.357 Å, the concomitant elongation of the other Fe–O bond by 0.104 Å and the elongation of one of the C–O bonds by 0.779 Å. Moreover, the O–Fe–O bond angle becomes larger by 17.3°. The predicted low activation barrier for the reduction of CO_2 to CO with ground-state Fe atoms following pathway (**b**) also indicates that both pathways should be competitive with a slight preference to pathway (**a**). It is worth noting that the product OFe(η^1-**O**C), **9**, can be easily converted to the more stable isomeric product OFe(η^1-**C**O), **7**, according to the mechanism discussed below.

Coordination Modes of CO to Ground-State Diatomic FeO and the Respective Isomerization Process

Searching the PES of the [FeO,CO] system, we located structure OFe(η^1-**O**C), **9**, at 10.40 (28.23) kcal/mol higher in energy with respect to the global minimum **7**. Complex **9** is easily converted to intermediate **10** through transition state **TS910** surmounting a barrier of 9.35 (8.68) kcal/mol (Fig. 6). The intermediate **10** involving coordination of the CO ligand to Fe atom in a "side-on" or η^2-CO bonding mode is more stable than **9** by 25.44 (23.03) kcal/mol, but it is less stable than the global minimum **7** by 11.11 (19.70) kcal/mol. Obviously, the preferred bonding mode of the CO ligand to the Fe end of the FeO molecule follows the trend: η^1-**C**O > η^2-**CO** > η^1-**O**C. In turn, the OFe(η^2-**CO**) intermediate is further converted to the final product **7** through transition state **TS107** in an almost barrier-less process; the activation barrier is only 3.14 (1.96) kcal/mol. The imaginary frequencies of **TS910** and **TS107** at 314i and 244i cm^{-1} correspond to the bending of the FeOC and FeCO moieties, respectively. The normal coordinate vectors (ar-

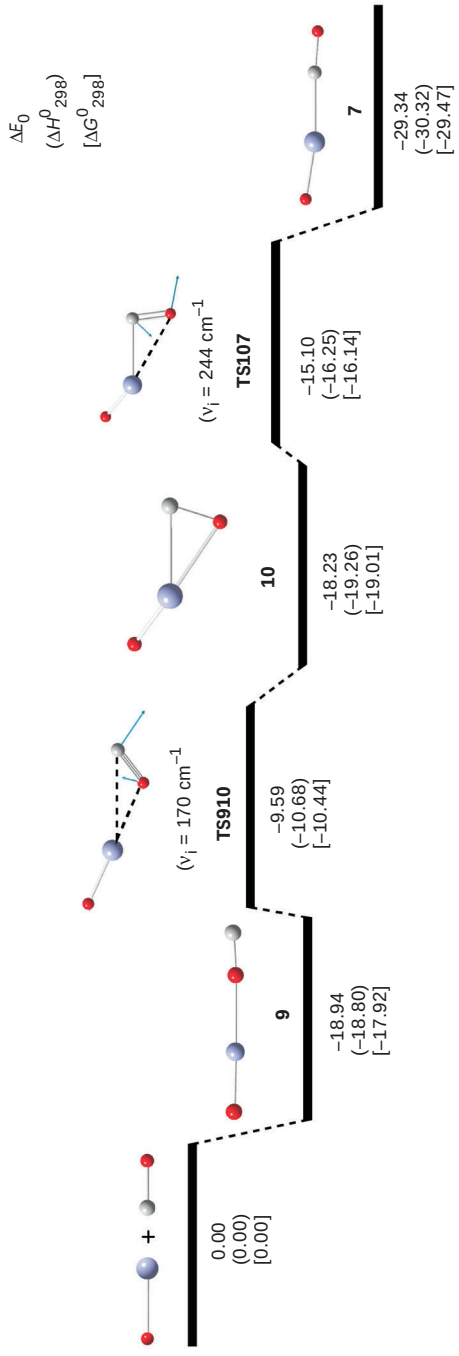

FIG. 6
Equilibrium structures (bond lengths in Å, bond angles in °) of the stationary points located on the PES of the [FeO,CO] system computed at the B3LYP/6-31G(d) level of theory

rows) of the vibrational modes are shown in Fig. 6. The IRC calculations at the B3LYP/6-31G(d) level of theory confirmed that **TS910** and **TS107** connect the respective reactants and products. Both **TS910** and **TS107** correspond to reactant-like transition states exhibiting some structural changes related to the elongation of the η^1-coordinated Fe–OC bond by 0.040 and 0.415 Å, respectively, and the narrowing of the O–Fe–C angle by 29.9 and 9.3°, respectively.

Let us now go deeper into the electronic features accounting for the relative stability of the Fe(η^1-**C**O), Fe(η^2-**CO**), and Fe(η^1-**O**C) bonding modes in the [FeO,CO] system. The Fe atom acquires a positive natural charge of 0.87, 0.82 and 1.26 charge units in **7**, **9** and **10**, respectively. The computed bond overlap populations of the Fe–C bond in **7**, the Fe–O bond in **9** and the Fe–C and Fe–O bonds in **10** are 0.133, –0.016, 0.153 and 0.074, respectively. Obviously, the Fe···O interaction in **9** is very weak, while in **10** the Fe–C and Fe–O interactions seem to be stronger than the corresponding interactions in **7** and **9**. This could be the result of the synergic bonding in the η^2-**CO** bonding mode involving both the σ-dative and the π-back bonding interactions. The total atomic spin densities of the three complexes shown in Scheme 2 are delocalized on the Fe and O atoms of the FeO moiety; the spin density values on the Fe and O atoms in **7** are 3.202 and 1.048, those in **9** are 3.447 and 0.519 and those in **10** are 3.665 and 0.5170, respectively. Moreover, the natural electron configuration of Fe is $4s^{0.84}3d^{6.20}$, $4s^{1.05}3d^{6.01}$ and $4s^{0.42}3d^{6.22}$ in complexes **7**, **9** and **10**, respectively. Finally,

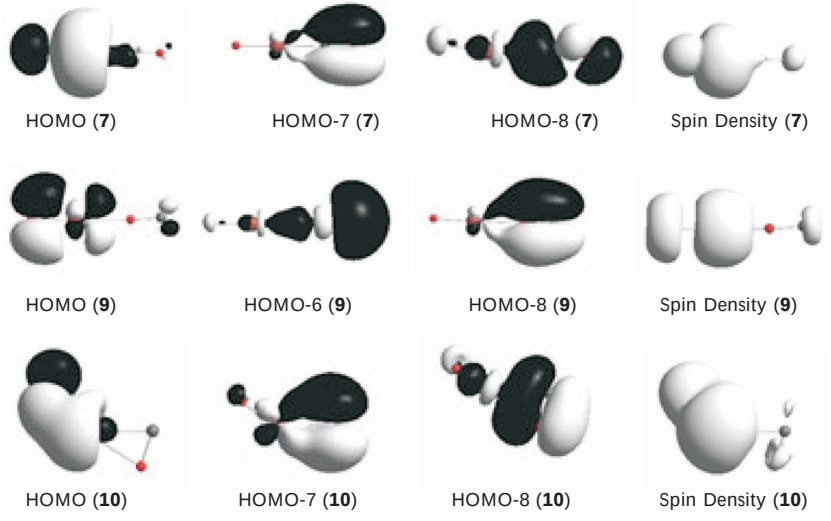

SCHEME 2

the relevant orbital interactions characterizing the bonding mode of the CO ligand to FeO molecule are depicted schematically in Scheme 2.

Vibrational Spectra of the [Fe,CO_2] and [FeO,CO] Systems

Considering that the mostly used experimental method in the characterization of the various species formed in the reaction between laser-ablated metal atoms and CO_2 or the co-condensation of metal atoms with CO_2 in net matrices at 15 K is FTIR, we calculated the vibrational spectra of all possible species involved in the Fe + CO_2 → FeO + CO reaction. The harmonic

TABLE II
Harmonic vibrational frequencies (in cm^{-1}) of the stationary points found in the PES of the [Fe,CO_2] system computed at the B3LYP/6-31G(d) level of theory

Species	Frequency					
	γ($FeCO_2$)	ν(Fe–O)	ν(Fe–C)	δ(OCO)	ν_{sym}(C=O)	ν_{as}(C=O)
1	6		16	636	1371	2434
				638		
2	9	21		639	1372	2435
	10			639		
3	62		64	560	1364	2419
				619		
4	285		326	696	1506	
	367[a]			1068[b]		
TS35	–245[c]			430	1261	2266
	134			520		
5	257		374	450[a]	1159	2008
				663		
6		297[d]	383[a]	722	1246	1533
		306[e]				
TS36		–271[d]	436[a]	471	1254	2037
		84[e]				
TS69	175	–250[f]	227[d]		840	1804
			475[g]			

[a] Out-of-plane $FeCO_2$. [b] Skeletal $FeCO_2$. [c] δ(OFeC). [d] ν_{sym}(OFeO). [e] ν_{as}(OFeO). [f] ν(C···O). [g] δ(FeOC).

vibrational frequencies of all stationary points found in the PES of the [Fe,CO_2] and [FeO,CO] systems computed at the B3LYP/6-31G(d) level of theory along with their assignment are given in Tables II and III, respectively. The most characteristic bands, which can be used to distinguish between the η^2-**OC**O, η^3-**OCO** and η^1-O**C**O coordination modes of the CO_2 ligand to the ground-state Fe metal center are those related to the coordinated CO_2 ligand, namely the ν_{as}(C=O), ν_{sym}(C=O) and δ(OCO) vibrational modes. In the η^2-CO bonding mode (complex **5**), the ν_{as}(C=O) vibration absorbs at much higher frequencies (2008 cm^{-1}) than in the η^3-**OCO** (complex **6**) coordination mode (1533 cm^{-1}), while it is absent in the η^1-C coordination mode (complex **4**). Moreover, the ν_{as}(C=O) – ν_{sym}(C=O) separation is 849 and 287 cm^{-1} for the η^2-**OC**O and η^3-**OCO** coordination modes, respectively. The experimentally observed vibrational frequencies at 1565 and 1210 cm^{-1} for the co-condensation reaction products of Fe atoms with CO_2

TABLE III

Harmonic vibrational frequencies (in cm^{-1}) of the stationary points found in the PES of the [FeO,CO] system computed at the B3LYP/6-31G(d) level of theory

Species	Frequency				
	skeletal	δ(FeCO)	ν(FeC)	ν(Fe=O)	ν(C=O)
7	85	167	374	943	2117
			392		
8	–33	363	460	693	2115
	53	–395			
TS57	225	305	457	858	2059
9	85		212[a]	1000	2121
	172				
10	130		350[a]	979	1779
	163		412		
TS910	106	–170	265[a]	981	1969
		133[b]			
TS107	84	–244	378	960	1946
		147[c]			

[a] ν(Fe–O). [b] δ(OFeO). [c] δ(OFeC).

at 15 K match those of the Fe(η^3-**OCO**) product, thereby excluding the formation of the proposed Fe(η^1-O**C**O) complex[5c]. The δ(OCO) vibrational mode is not so sensitive to the coordination mode of the CO_2 ligand. Thus, δ(OCO) is 663, 722 and 696 cm^{-1} for the η^2-**OC**O, η^3-**OCO** and η^1-O**C**O bonding modes, respectively.

Finally, the most characteristic bands, which can be used to distinguish between the η^1-**C**O, η^1-**O**C and η^2-**CO** coordination modes of the CO ligand to the ground-state FeO moiety are the ν(C≡O) and ν(Fe=O) vibrational modes. In the η^1-**C**O bonding mode (complex **7**), the ν(C≡O) and ν(Fe=O) vibrations absorb at 2117 and 943 cm^{-1}, in the η^1-**O**C (complex **9**) at 2121 and 1000 cm^{-1} and in the η^2-**CO** (complex **10**) coordination mode at 1779 and 979 cm^{-1}, respectively. It is worth noting that the computed ν(C≡O) and ν(Fe=O) vibrational frequencies at 2117 and 943 cm^{-1} for **7** compare well with the experimentally observed ν(C≡O) and ν(Cr=O) vibrational frequencies at 2014.4 and 866.3 cm^{-1} for the insertion product OCrCO formed upon interaction of Cr atoms generated by laser ablation with CO_2 (ref.[22]).

CONCLUSIONS

A detailed investigation of the mechanism of the CO_2-to-CO reduction by ground-state Fe atoms has been carried out in the framework of electronic structure calculations at the B3LYP level of theory, using the 6-31G(d) and 6-311+G(3df) basis sets.

The Fe + CO_2 → FeO + CO reaction is predicted to be endothermic by 23.24 kcal/mol at the B3LYP/6-311+G(3df)//B3LYP/6-31G(d) level of theory. The reaction could follow two possible alternative pathways (**a**) or (**b**) depending on the nature of the entrance channel involving formation of either an Fe(η^2-**OC**O) or an Fe(η^3-**OCO**) intermediate.

The Fe(η^2-**OC**O) intermediate was found to be weakly bound with respect to Fe(^{5}D) and CO_2 dissociation products by only 0.78 (2.88) kcal/mol at the B3LYP/6-31G(d) (B3LYP/6-311+G(3df)//B3LYP/6-31G(d)) levels of theory, but strongly bound relative to the separated Fe^+(^{6}D) and $[CO_2]^-$ anion; the computed Fe–CO_2 bond dissociation energy is predicted to be 207.33 kcal/mol in terms of ΔE_0 at the B3LYP/6-31G(d).

On the other hand, the Fe(η^3-**OCO**) intermediate is unbound with respect to Fe(^{5}D) and CO_2 dissociation products by 8.27 (11.15) kcal/mol at the same levels of theory, but also strongly bound relative to the separated Fe^+(^{6}D) and $[CO_2]^-$ anion; the computed Fe–CO_2 bond dissociation energy is predicted to be 198.28 kcal/mol.

Both reaction pathways involve an intramolecular insertion reaction of the Fe atom into the O–C bond of the Fe(η^2-**OC**O) and Fe(η^3-**OCO**) intermediates yielding the isomeric OFe(η^1-**C**O) and OFe(η^1-**O**C) insertion products, respectively, with a relatively low activation barrier of 25.24 (21.69) and 26.36 (23.38) kcal/mol at the B3LYP/6-31G(d) (B3LYP/6-311+G(3df)//B3LYP/6-31G(d)) levels of theory, respectively. The predicted activation barriers for the reduction of CO_2 to CO with ground-state Fe atoms following either pathway (**a**) or (**b**) indicate that both pathways should be competitive with a slight preference to pathway (**a**).

Finally, the ligation modes of the CO_2 ligand (η^3-**OCO**, η^2-**OC**O ("side-on"), η^2-**O**C**O**, η^1-**O**CO, and η^1-O**C**O) to the ground-state Fe metal center along with the ligation modes of CO to the ground-state FeO diatomic have exhaustively been explored at the B3LYP/6-31G(d) and B3LYP/6-311+G(3df)//B3LYP/6-31G(d) levels of theory and are discussed with respect to computed electronic and spectroscopic properties, such as charge density distribution and harmonic vibrational frequencies.

REFERENCES

1. Yin X., Moss J. R.: *Coord. Chem. Rev.* **1999**, *181*, 27; and references therein.
2. Herskovitz T.: *J. Am. Chem. Soc.* **1977**, *99*, 2391.
3. Behr A.: *Carbon Dioxide Activation by Metal Complexes*. VCH, Weinheim 1988.
4. a) Braunstein P., Matt D., Nobel D.: *Chem. Rev.* **1988**, *88*, 747; b) Behr A.: *Angew. Chem., Int. Ed. Engl.* **1988**, *27*, 661.
5. a) Ozin G. A., Huber H., McIntosh D.: *Inorg. Chem.* **1978**, *17*, 1472; b) Huber H., McIntosh D., Ozin G. A.: *Inorg. Chem.* **1977**, *16*, 975; c) Mascetti J., Tranquille M.: *J. Phys. Chem.* **1988**, *92*, 2177; d) Galan F., Fouassier M., Tranquille M., Mascetti J., Pápai I.: *J. Phys. Chem. A* **1997**, *101*, 2626.
6. a) Tjelta B. L., Walter D., Armentrout P. B.: *Int. J. Mass Spectrom.* **2001**, *204*, 7; b) Gregoire G., Velasquez J., Duncan M. A.: *Chem. Phys. Lett.* **2001**, *349*, 451; c) Dieterle M., Harvey J. N., Heinemann C., Schwarz J., Schröder D., Schwarz H.: *Chem. Phys. Lett.* **1997**, *277*, 399; d) Asher R. L., Bellert D., Buthelezi T., Brucat P. J.: *Chem. Phys. Lett.* **1995**, *243*, 269; e) Schwarz J., Schwarz H.: *Organometallics* **1994**, *13*, 1518; f) Lesson D. E., Asher R. L., Brucat P. J.: *J. Chem. Phys.* **1991**, *95*, 1414.
7. Caballol R., Marcos E. S., Barthelat J.-C.: *J. Chem. Phys.* **1987**, *91*, 1328.
8. Jeung G.-H.: *Chem. Phys. Lett.* **1995**, *232*, 319.
9. Hwang D.-Y., Mebel A. M.: *Chem. Phys. Lett.* **2002**, *357*, 51.
10. a) Pápai I., Hannachi Y., Gwizdala S., Mascetti J.: *J. Phys. Chem. A* **2002**, *106*, 4181; b) Pápai I., Schubert G., Hannachi Y., Mascetti J.: *J. Phys. Chem. A* **2002**, *106*, 9551; c) Pápai I., Mascetti J., Fournier R.: *J. Phys. Chem. A* **1997**, *101*, 4465.
11. Fan H.-J., Liu C.-W.: *Chem. Phys. Lett.* **1999**, *300*, 351.
12. Sodupe M., Branchandell V., Rosi M., Bauschlicher C. W., Jr.: *J. Phys. Chem. A* **1997**, *101*, 7854.

13. a) Becke A. D.: *Phys. Rev. A: At., Mol., Opt. Phys.* **1988**, *38*, 3098; b) Vosko S. H., Wilk L., Nussair M.: *Can. J. Phys.* **1980**, *58*, 1200; c) Becke A. D.: *J. Chem. Phys.* **1993**, *98*, 5648.
14. Lee C., Yang W., Parr R. G.: *Phys. Rev. B: Condens. Matter* **1988**, *37*, 785.
15. a) Ziegler T.: *Chem. Rev.* **1991**, *91*, 651; b) Nicholas J. B.: *Top. Catal.* **1997**, *4*, 157; c) Koch W. R., Hertwing H.: *Chem. Phys. Lett.* **1997**, *286*, 345; d) Curtis L. A., Raghavachari K., Redfern P. C., Pople J. A.: *Chem. Phys. Lett.* **1997**, *270*, 419; e) Smith D. M., Golding B. T., Radom L.: *J. Am. Chem. Soc.* **1999**, *121*, 9388; f) Chandra A. K., Nguyen M. T.: *Chem. Phys.* **1998**, *232*, 299; g) Mire L. W., Wheeler S. D., Wagenseller E., Marynick D. S.: *Inorg. Chem.* **1998**, *37*, 3099; h) Nicholas J. B.: *Top. Catal.* **1999**, *9*, 181; i) Arnaud R., Adamo C., Cossi M., Millet A., Vallé Y., Barone V.: *J. Am. Chem. Soc.* **2000**, *122*, 324.
16. Schlegel H. B.: *J. Comput. Chem.* **1982**, *3*, 214.
17. Head-Gordon M., Pople J. A., Frisch M.: *Chem. Phys. Lett.* **1988**, *153*, 503.
18. a) Gonzalez C., Schlegel H. B.: *J. Chem. Phys.* **1989**, *90*, 2154; b) Gonzalez C., Schlegel H. B.: *J. Phys. Chem.* **1990**, *94*, 5523.
19. Frisch M. J., Trucks G. W., Schlegel H. B., Scuseria G. E., Robb M. A., Cheeseman J. R., Zakrzewski V. G., Montgomery J. A., Stratmann R. E., Burant J. C., Dapprich S., Millam J. M., Daniels A. D., Kudin K. N., Strain M. C., Farkas O., Tomasi J., Barone V., Cossi M., Cammi R., Mennucci B., Pomelli C., Adamo C., Clifford S., Orchterski J., Petersson G. A., Ayala P. Y., Cui Q., Morokuma K., Malick D K., Rabuck A. D., Raghavachari K., Foresman J. B., Cioslowski J., Ortiz J. V., Baboul A. G., Stefanov B. B., Liu G., Liashenko A., Piskorz P., Komaroni I., Gomperts R., Martin R. L., Fox D. J., Keith T., Al-Laham M. A., Peng C. Y., Nanayakkara A., Gonzalez C., Challacombe M., Gill P. M., Johnson P., Chen W., Wong M. W., Andres J. L., Head-Gordon M., Replogle E. S., Pople J. A.: *Gaussian 98*, Revision A.7. Gaussian Inc., Pittsburgh (PA) 1998.
20. ChemOffice 97 Cambridge Scientific Computing, Inc., 875 Massachusetts Ave., Suite 41, Cambridge, MA 02139, U.S.A.
21. *NIST Chemistry Webbook*. NIST Standard Reference Data Base Number 9, February 2000 Release (http://webbook.nist.gov/chemistry/).
22. Souter P. F., Andrews L.: *J. Am. Chem. Soc.* **1997**, *119*, 7350.